

See discussions, stats, and author profiles for this publication at: <https://www.researchgate.net/publication/256375847>

# Anisotropic Structure and Charge Transport in Highly Strain-Aligned Regioregular Poly(3-hexylthiophene)

ARTICLE *in* ADVANCED FUNCTIONAL MATERIALS · OCTOBER 2011

Impact Factor: 11.81 · DOI: 10.1002/adfm.201100904

---

CITATIONS

51

READS

59

## 6 AUTHORS, INCLUDING:



Brendan O'Connor

North Carolina State University

25 PUBLICATIONS 510 CITATIONS

[SEE PROFILE](#)



Brad R. Conrad

Appalachian State University

37 PUBLICATIONS 291 CITATIONS

[SEE PROFILE](#)



Lee Richter

National Institute of Standards and Technology

166 PUBLICATIONS 6,028 CITATIONS

[SEE PROFILE](#)



David Gundlach

National Institute of Standards and Technology

137 PUBLICATIONS 7,702 CITATIONS

[SEE PROFILE](#)

# Anisotropic Structure and Charge Transport in Highly Strain-Aligned Regioregular Poly(3-hexylthiophene)

Brendan O'Connor, R. Joseph Kline, Brad R. Conrad, Lee J. Richter, David Gundlach, Michael F. Toney, and Dean M. DeLongchamp\*

A novel method of strain-aligning polymer films is introduced and applied to regioregular poly(3-hexylthiophene) (P3HT), showing several important features of charge transport. The polymer backbone is shown to align in the direction of applied strain resulting in a large charge-mobility anisotropy, where the in-plane mobility increases in the applied strain direction and decreases in the perpendicular direction. In the aligned film, the hole mobility is successfully represented by a two-dimensional tensor, suggesting that charge transport parallel to the polymer backbone within a P3HT crystal is strongly favored over the other crystallographic directions. Hole mobility parallel to the backbone is shown to be high for a mixture of plane-on and edge-on packing configurations, as the strain alignment is found to induce a significant face-on orientation of the originally highly edge-on oriented crystalline regions of the film. This alignment approach can achieve an optical dichroic ratio of 4.8 and a charge-mobility anisotropy of 9, providing a simple and effective method to investigate charge-transport mechanisms in polymer semiconductors.

## 1. Introduction

Semicrystalline polymer semiconductors are becoming a viable technology for large-area and low-cost electronic applications. While this technology continues to improve, the need to

fundamentally understand charge transport in these materials remains, which is a complex combination of transport through and between anisotropic crystalline and amorphous regions of the polymer.<sup>[1]</sup> Films with high levels of morphological anisotropy show features of charge transport that are difficult to distinguish in semicrystalline polymer films that are azimuthally isotropic (e.g., lacking in-plane orientation).<sup>[2,3]</sup> To obtain aligned conducting polymer films, there has been a range of approaches that include solution processing,<sup>[3–5]</sup> nanostructured confinement,<sup>[6]</sup> embossing,<sup>[7]</sup> rubbed or templated substrates,<sup>[8–15]</sup> direct rubbing of the active film,<sup>[16–18]</sup> directional solidification from a solvent or within a magnetic field,<sup>[2,19–21]</sup> and stretching or other physical deformation methods.<sup>[22–30]</sup> Here, we employ a method of straining the semicrystalline polymer, poly(3-hexylthiophene) (P3HT),

to align the polymer and gain insight into film morphology and charge-transport properties. The method introduced here can control the extent of polymer alignment, resulting in mobility anisotropies as high as 9. More importantly, this method enables the aligned film to be placed on an array of substrates for detailed morphological and electrical characterization without compromising film quality.

For any organic-semiconductor alignment method, it is critical to avoid introducing major film defects or other extrinsic effects that complicate attempts to understand the roles of various charge-transport processes, especially if the physical arrangement of those artifacts is related to the alignment. Previous alignment methods often suffer from the introduction of these extrinsic effects. Solution processing can often have a low level of alignment or gross film non-uniformities generated by the process.<sup>[4,5]</sup> Direct solidification can form sharp anisotropic grain boundaries that can dominate the charge-transport behavior, although it does permit studies of grain-boundary-driven transport anisotropy.<sup>[2,19]</sup> Alignment through substrate modification can adversely affect device performance, and often requires the semiconductor to pass through a liquid-crystalline phase.<sup>[6,9,31]</sup> Physically straining or shearing the polymer can achieve a high level of alignment; however previous applied methods resulted in poor performance relative to an as-cast film.<sup>[18,23]</sup>

Here, we demonstrate a method of strain alignment that has several advantages over previously demonstrated alignment

Dr. B. O'Connor,<sup>[+]</sup> Dr. R. J. Kline, Dr. D. M. DeLongchamp  
Polymers Division, National Institute of Standards and Technology  
Gaithersburg, MD 20899, USA

E-mail: deand@nist.gov

Dr. B. R. Conrad,<sup>[+,†]</sup> Dr. D. Gundlach  
Semiconductor Electronics Division  
National Institute of Standards and Technology  
Gaithersburg, MD 20899, USA

Dr. L. J. Richter  
Surface and Microanalysis Division  
National Institute of Standards and Technology  
Gaithersburg, MD 20899, USA

Dr. M. F. Toney  
Stanford Synchrotron Radiation Lightsource  
Menlo Park, CA 94025, USA

[+] Present Address: Department of Mechanical and Aerospace  
Engineering, North Carolina State University, Raleigh, NC 27695, USA

[†+] Present Address: Department of Physics and Astronomy, Appalachian State University, Boone, NC 28608, USA

DOI: 10.1002/adfm.201100904

schemes. The polymer test film to be strained is first cast upon an octyltrichlorosilane-modified oxidized silicon (OTS-Si) substrate. The film is then transferred to polydimethylsiloxane (PDMS) and the PDMS-test film composite is strained to varying extents. While the composite is held under strain, the test film is transferred to a range of secondary substrates for detailed morphological and electronic characterization. The PDMS transfer process is similar to that previously reported by Chabynic et al.<sup>[32]</sup> This method provides three critical advantages over other strain-alignment processes. First, the film can be cast on a substrate that promotes optimal morphology.<sup>[33]</sup> Second, the test-film surface that ultimately contacts the dielectric is free of contact throughout the alignment process, and the other transistor elements—the dielectric and electrodes—are not strained. Finally, this method enables one to place the strained film on a wide variety of substrates for detailed characterization of both the morphology and electronic properties. In this report, we investigate the morphology of highly strain-aligned P3HT films in detail, followed by tests of the strained films in organic thin-film transistors (OTFTs) to probe the anisotropy of their electronic properties.

## 2. Results and Discussion

### 2.1. Morphological Anisotropy

To investigate the morphology of the strained film, we begin by measuring the topography of the films with atomic force microscopy (AFM). In Figure 1, the topography of a spin-coated film is compared to PDMS-transferred films strained to varying extents. The spin-coated film, with a root mean square (RMS) roughness of  $\approx 1.2$  nm is considerably smoother than the unstrained PDMS transferred film, which has an RMS roughness of  $\approx 3.6$  nm. When strain is applied to the P3HT-PDMS composite, the transferred P3HT film becomes smoother but remains rougher than the initial cast film. The increased roughness of the P3HT film is likely related to conformal contact with the PDMS surface and possibly a non-uniform adhesion to PDMS during film transfer and PDMS removal. We believe that the polymer surface that contacts the secondary substrate remains smooth. As the film is strained, the development of fibrils roughly in the direction of applied strain are also observed. The fibrils exhibit greater lengths than would be expected purely by stretching the rough topography of the film. Importantly, the strained P3HT films show no signs of cracking, and the films remain continuous at strains greater than 150%. This limit in the level of applied strain is due to failure of the PDMS host, which ruptured between 130 and 170% strain.

### 2.1.1. Molecular Orientation

Because the primary optical transition for P3HT has a transition dipole moment ( $\pi-\pi^*$ ) that is parallel to the polymer backbone long axis,<sup>[34]</sup> the extent of polymer chain alignment can be evaluated by measuring polarized optical absorbance. P3HT films strained to varying extents were transferred to a glass substrate and placed in an ultraviolet-visible (UV-vis) spectrometer equipped with a rotating polarizer. The dichroic ratio,  $R = A_{\parallel}/A_{\perp}$ , where  $A$  is the absorbance of the film with polarized light parallel ( $\parallel$ ) and perpendicular ( $\perp$ ) to the strain direction at the peak absorption wavelength of the parallel polarized light is shown in Figure 2. Under strain, the films show a clear optical anisotropy with  $R$  linearly dependent on the level of applied strain. With the  $\pi-\pi^*$  transition parallel to the backbone of the polymer, the dichroic ratio shows a significant extent of backbone alignment in the direction of strain. With increasing applied strain, there is also a change in the absorption spectra in both the parallel and perpendicular directions. In Figure 2, the absorbance peaks are normalized to highlight the changes in the absorbance spectra, absolute absorbance results are provided in the Supporting Information. Parallel to the applied strain direction, absorbance features at 605 and 550 nm become more prominent with increasing strain. Perpendicular to the applied strain direction, there is no change in the absorbance character at low strain; however at high strain the features at 605

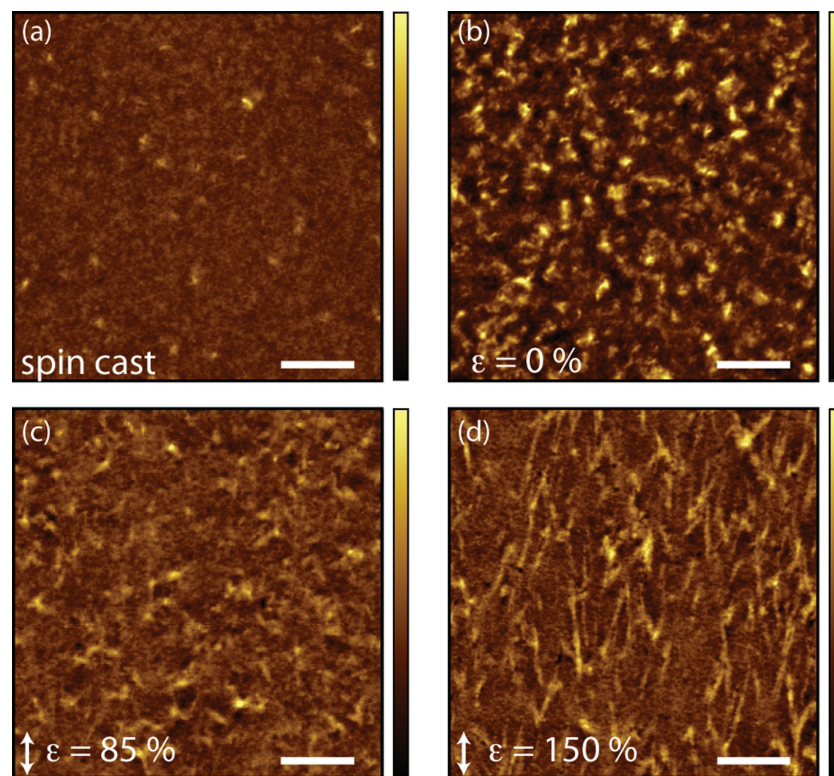


**Figure 1.** AFM images of P3HT films on silicon substrates under different processing conditions: a) spun cast P3HT film on an OTS-modified silicon substrate (RMS roughness = 1.2 nm), b) PDMS transferred film with 0% applied strain (RMS = 3.6 nm), c) PDMS transferred film with 85% applied strain (RMS = 2.3 nm); d) PDMS transferred film with 150% applied strain (RMS = 2.7 nm). The applied strain is given in the bottom left corner of the figure for both strained films. The scale bar on all microscopy images is 2  $\mu$ m, the z-scale bar is 25 nm for all films.

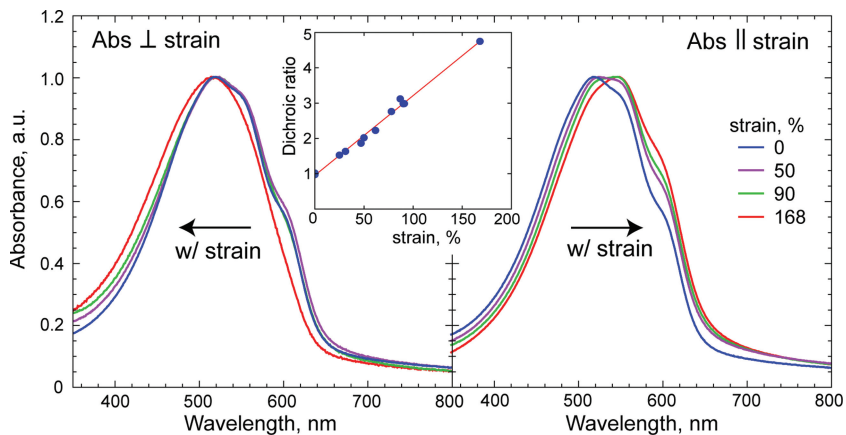


**Figure 2.** Normalized absorbance of P3HT films under varying levels of strain. All absorbance curves are normalized by the maxima of the spectra. Left: absorbance with light polarized perpendicular to the strain direction. Right: absorbance with light polarized parallel to the strain direction. Inset: dichroic ratio of the P3HT films over a range of strains, with a linear fit to the data.

and 550 nm are lost. These features arise from a complex interplay between intramolecular vibronic coupling (giving rise to a Franck–Condon series with the 0→0 transition near 605 nm) and intermolecular, H-aggregate-like, coupling.<sup>[35]</sup> Qualitatively, resolution of the vibronic series is indicative of good local conformational order. Quantitatively, the ratio of the 0→0 transition intensity (near 605 nm) to the 0→1 transition intensity (near 550 nm) has been related to the intermolecular (H-aggregate) band width.<sup>[35]</sup> The changes in the spectra for polarization parallel to strain suggest slight improvements in local order and an increase in the intermolecular band width (increase in the relative 0→0 intensity); however, the change in peak intensities is not large compared to what can be achieved through other processing avenues, and the overall increase in conformational order is modest.<sup>[35]</sup> Similarly, perpendicular to strain, the evolution of the spectra is consistent with a modest loss of local order and decrease in intermolecular band width (decrease in relative 0→0 intensity).

To further examine whether reorienting the polymer changes the extent of conformational order, variable-angle spectroscopic ellipsometry (VASE) was performed on a 0 and 100% strained film (see the Supporting Information, Figure S2). A diagonal biaxial dielectric function was assumed, consistent with the  $C_{2v}$  symmetry of the applied strain. Both dielectric function and film thickness were determined. When the P3HT films are strained they become thinner; however, the total volume of P3HT is conserved, indicating predominantly plastic deformation. The original unstrained films are anisotropic (uniaxial, unique axis along surface normal: z). The major effect of strain is to break the degeneracy in the xy plane; however, strain additionally

decreases the out-of-plane component of the dielectric function. If strain simply reorients anisotropic chromophores in the film, with no change in local order, the trace of the dielectric tensor should be conserved. The trace of the dielectric integrated between 400 and 600 nm for the unstrained film and for the 100% strained film differed by less than 4%, suggesting that the extent of order within the polymer is not substantially changed with alignment. Together, the UV-vis spectroscopy and VASE measurements imply that the polymer is comprehensively reoriented with only a modest increase in its extent of local conformational order.

### 2.1.2. Crystal Orientation

To probe the behavior of the crystalline regions of the film, strained films were transferred to silicon substrates and measured using X-ray diffraction. Two-dimensional (2D) grazing-incidence X-ray diffraction (GIXD) patterns are provided in Figure 3 for an unstrained film and films strained by 95 and 140%. GIXD in-plane line scans from a point-detector geometry are provided in Figure 4 for a series of films strained from 0 to 112%. For the unstrained film, the scattering pattern is independent of

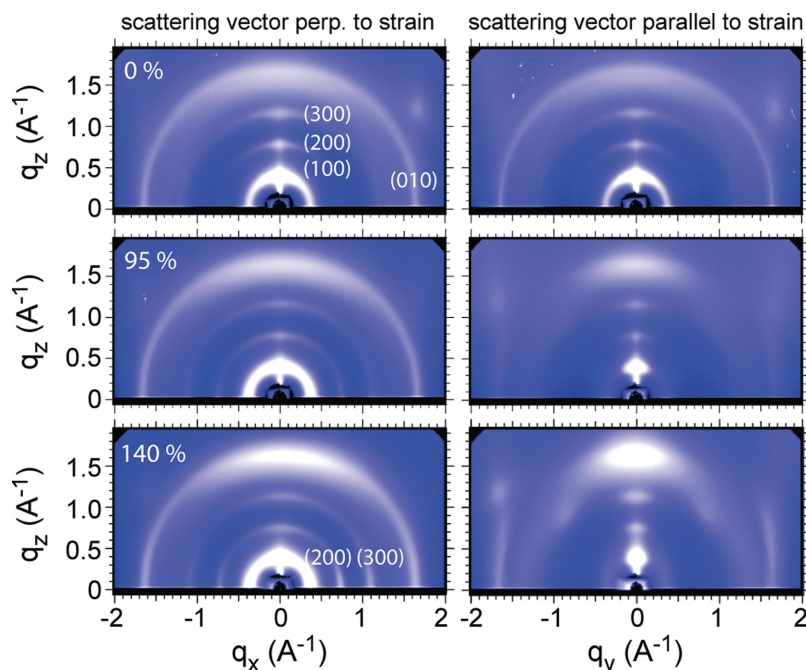


**Figure 3.** 2D-GIXD images collected with an area detector with the left panel for the scattering vector nominally perpendicular to the strain direction (incident X-ray beam parallel to strain), and the right panel for the scattering vector nominally parallel to the strain direction (incident X-ray beam perpendicular to strain). Images are for films strained by 0, 95, and 140%. The indexed lattice planes are defined in the inset schematic provided in Figure 5. Note that the incident beam and scattering vector are not perpendicular to each other. The scattering vector deviates from normal by  $\theta_B$ , but the difference is less than the FWHM of the in-plane orientation distribution.

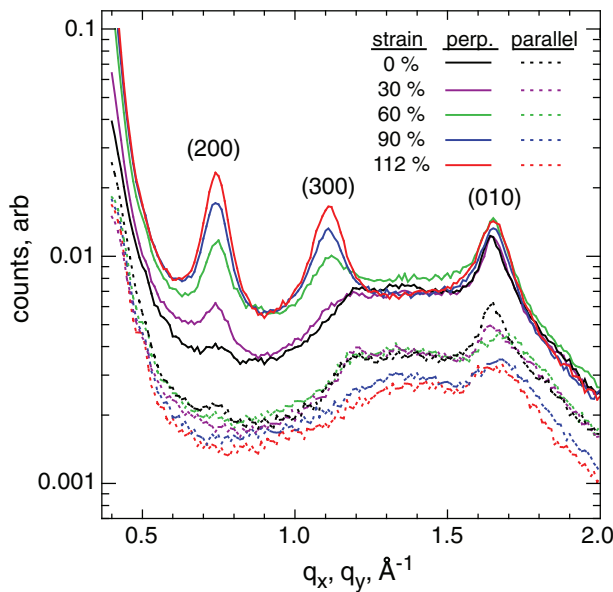


**Figure 4.** High-resolution GIXD line-scans for P3HT films of various strain with the scattering vector oriented perpendicular and parallel to the strain direction, respectively. For this geometry, unlike the image plate data, the incident X-ray beam is *not* parallel and perpendicular to the strain direction. The in-plane orientation of the sample to the X-ray beam is adjusted for each scattering vector ( $\mathbf{q}$ ) position to maintain the scattering vector perpendicular or parallel to the strain direction. Note that the line-scan background signal changes with strain and beam direction due to asymmetry of the film area.

the in-plane scattering vector orientation and similar to previously reported P3HT films cast on an OTS–Si substrate with a preferential edge-on orientation and an isotropic in-plane orientation distribution.<sup>[36]</sup> For the strained films, a clear anisotropy develops. When the scattering vector was nominally perpendicular to the strain direction (the incident beam aligned roughly along the strain direction), the (100) peak in the surface plane increased relative to the unstrained film (an increase in the amount of plane-on crystals with the backbone in the direction of applied strain). When the scattering vector was nominally parallel to the strain direction (the incident beam aligned roughly perpendicular to the strain direction), weak scattering near the position of the (010) peak is observed while the in-plane (100) peak is reduced considerably. The out of plane peaks (h00) along the meridian in Figure 3 are similar in both incident-beam directions due to their insensitivity to beam in-plane orientation. It should also be noted that the measured  $d$ -spacings for the alkyl and  $\pi$ -planes are independent of strain.

When the scattering vector is perpendicular to the strain direction, the X-ray diffraction intensity associated with plane-on crystals increases, whereas that associated with the edge-on crystals stays relatively constant. This is likely due to edge-on crystals rotating about the crystalline  $c$  axis towards plane-on during strain-induced alignment. Edge-on crystals with their backbones already parallel to the direction of strain would remain unchanged. These results are consistent with near-edge X-ray absorption fine spectroscopy (NEXAFS), which shows that the bottom-surface orientation of the P3HT (the surface in

contact with the dielectric layer in a transistor configuration) is increasingly plane-on for polymer chains oriented in the direction of strain (see the Supporting Information). Note that in the direction perpendicular to strain, the  $q_y$  peak near  $1.65 \text{ \AA}^{-1}$  is attenuated and shifts towards higher  $q$  and broadens (visible in both Figure 3 and Figure 4). The scattering at this position in reciprocal space in unaligned films is primarily due to (010)  $\pi$ -stacking from edge-on polymers, but has been reported to include a contribution from the (002) lattice plane vector along the polymer backbone.<sup>[2]</sup> Our alignment process reorients the majority of (010) in-plane scattering and allows the underlying weaker backbone scattering to be observed in the perpendicular direction. This shift in  $q$  is not due to a change in the unit cell of the polymer, but rather the emergence of a scattering peak other than the (010).

To measure the relative orientation distribution of the crystalline portion of the polymer,  $\varphi$ -scans were performed on films a varying strain, provided in Figure 5 and Figure S4. A  $\varphi$ -scan is performed by measuring the diffraction intensity at a specific point in  $\mathbf{q}$  [here the in-plane lamella stacking peak (200)], and rotating the sample about the surface normal, revealing the in-plane orientation distribution. For a film strained by 112%, the  $\varphi$ -scan shows that plane-on crystals have a distribution with a peak in the strain direction and a FWHM of approximately 20°. To quantify the degree of orientation of the crystalline material, we apply a 2D order parameter ( $S_2$ ) to the X-ray  $\varphi$ -scan defined as,<sup>[21,37]</sup>

$$S_2 = 2 \langle \cos^2(\varphi) \rangle - 1 \quad (1)$$

with  $\langle \cos^2(\varphi) \rangle$  for an order parameter of the crystalline material ( $S_{2,\text{cryst}}$ ) given by,

$$\langle \cos^2(\varphi) \rangle = \frac{\int_0^\pi I(\varphi) \cos^2(\varphi) d\varphi}{\int_0^\pi I(\varphi) d\varphi} \quad (2)$$

where  $I(\varphi)$  is the X-ray scattering intensity at a given  $\varphi$ ; for complete alignment  $S = 1$ , whereas for unoriented material  $S = 0$ . A 2D order parameter is appropriate because the VASE indicates the polymer chains are largely constrained to the plane of the film. From the  $\varphi$ -scan depicted in Figure 5, a 112% strained film,  $S_{2,\text{cryst}} = 0.84$ , demonstrates a high level of crystal orientation. Assuming that the  $\varphi$ -scan of the plane-on crystals is representative of the distribution of all crystalline material, the crystal orientation can be compared to molecular orientation (both crystal and amorphous material) by considering the optical dichroic ratio. The orientation parameter of the entire film based on absorbance is also given by Equation 1, which can be put in terms of the dichroic ratio (derived in the Supporting Information) and given by,

$$S_{2,\text{mol}} = \frac{R - 1}{R + 1} \quad (3)$$

For a film strained by 112% (consistent with the  $\varphi$ -scan)  $R$  is approximately 3.5 and  $S_{2,\text{mol}} = 0.56$ . The difference between

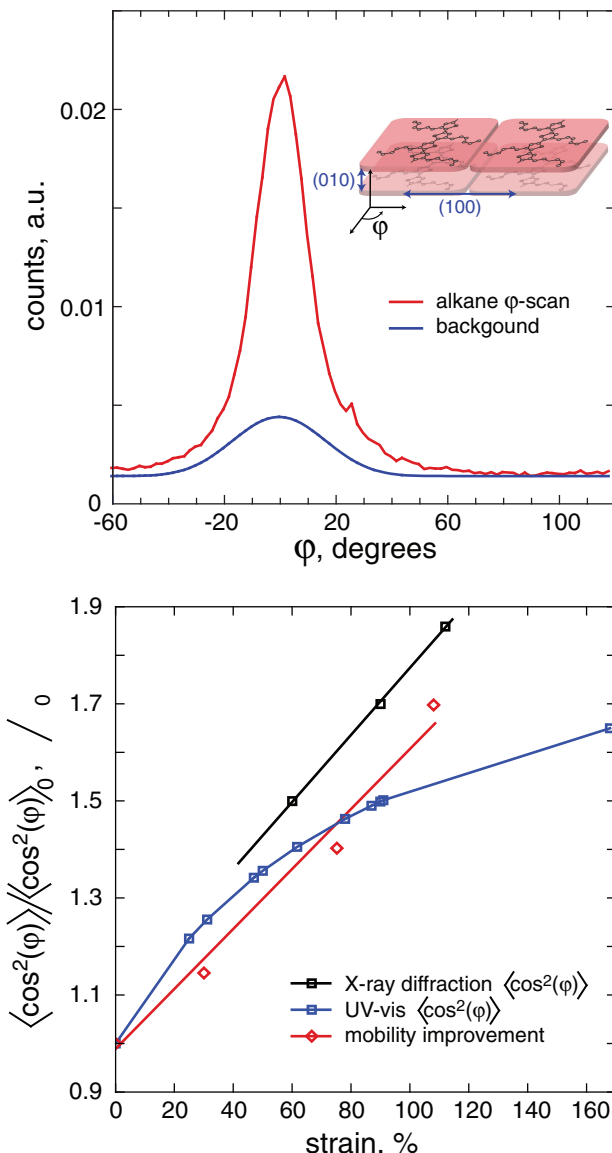


**Figure 5.** Top: X-ray diffraction  $\phi$ -scan of the in-plane (200) alkane side chain stacking peak for a film strained by 112%. The background is an estimate of the background signal of the X-ray beam that occurs due to the film geometry and is based on the line scans in Figure 4 (see the Supporting Information for additional details). Inset: schematic of the  $\phi$ -scan orientation and structure of the crystalline film being probed, where 0 is the direction of applied strain. Bottom: average orientation of the polymer backbone as measured by X-ray diffraction and UV-vis spectroscopy under varying levels of strain, normalized by the average orientation of an isotropic film (i.e.,  $\langle \cos^2(\phi) \rangle_0 = 0.5$ ). Also plotted is the saturated charge mobility in the direction of applied strain for 5- $\mu\text{m}$  channel-length transistors, normalized by the mobility at 0% strain ( $\langle \rangle_0$ ). Line fits are applied to the X-ray diffraction and mobility data.

the molecular order parameter ( $S_{2,\text{mol}}$ ) and the crystalline one ( $S_{2,\text{cryst}}$ ) can be explained by differences in the extent of chain alignment in the amorphous and the crystalline regions. If we assume that the amorphous material is isotropic, then the crystallinity of the film is approximately 64% (see the Supporting Information). This crystallinity is slightly larger than reported

estimates of  $\approx 50\%$ .<sup>[38]</sup> If we assume that the film is 50% crystalline, then  $S_2$  for the amorphous region is  $\approx 0.36$ .

The comparison of order parameters has a couple of key assumptions that should be highlighted. The crystalline order parameter does not account for edge-on crystals or any crystals with (100) orientation that are not in the plane of the film. It could change with knowledge of the full 3D orientation distribution, however this is a nontrivial measurement and beyond the scope of this work. Knowledge of the 3D crystal orientation distribution could either increase or decrease  $S_{2,\text{cryst}}$ . In addition, the molecular order parameter does not account for the difference in the absorbance spectrum in the two perpendicular directions of a strained film (due to differences in the intermolecular coupling of the polymer) and likely overestimates  $S_{2,\text{mol}}$ . While these assumptions preclude an exact measurement of the amorphous anisotropy, we nevertheless can conclude that that the amorphous material is not significantly oriented.

Summarizing the morphology of these films, we find that the films physically deform but are mechanically sound with no significant cracks. The crystalline material aligns in the direction of applied strain with the polymer backbone aligning proportionally to the amount of strain. There are minor improvements in conformational order of the polymer in the alignment direction, however major changes in overall film crystallinity are not observed. A significant feature of the reoriented crystalline material is that it prefers a plane-on configuration. The amorphous material remains largely isotropic in the strained films with minor levels of preferential backbone alignment in the direction of strain. A schematic overview of the polymer alignment is given in Figure 6.

## 2.2. Charge Transport Anisotropy

A key advantage of our strain alignment method is the ability to place the film on a range of substrates. We use this feature to measure charge transport by transferring the P3HT films onto the silicon oxide gate dielectric of bottom gate, bottom contact transistors. The test structure has transistors placed orthogonal to one another to probe the anisotropy of charge transport. The mobility of the P3HT films in the saturated operating regime is given in Figure 7 for films that have undergone varying amounts of strain. Note that a high mobility of  $0.05 \text{ cm}^2 \text{V}^{-1} \text{s}^{-1}$ , associated with OTS-treated dielectrics, is achieved when the film is transferred from an OTS-Si substrate to an unmodified silicon oxide gate dielectric, consistent with the work by Chabinyc et al.<sup>[32]</sup> The mobility increases along the direction of strain while decreasing in the perpendicular direction, with a maximum mobility anisotropy of 9. The majority of the charge-transport anisotropy occurs due to the decrease in mobility perpendicular to the applied strain direction, however a clear improvement is observed parallel to the applied strain (i.e., the direction of polymer backbone alignment). The improvement in mobility with applied strain compares well with the change in the average orientation ( $\langle \cos^2(\phi) \rangle$ ) of the (200) in-plane scattering peak, shown in Figure 5 and Figure 7.

To gain further insight into the charge transport anisotropy, the angular dependence of mobility for films strained to approximately 100% is provided in Figure 8, and is fit to the effective mobility,  $\langle \rangle_{\text{eff}} = \sum_j l_j l_j$ , where  $l_j$  is a 2-dimensional mobility tensor and  $l = [\cos(\theta), \sin(\theta)]$ .<sup>[39]</sup> The components of the

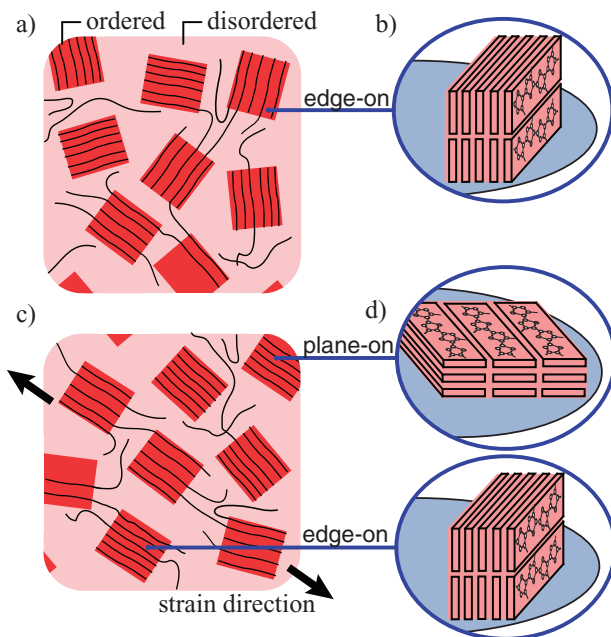


**Figure 6.** Schematic view of the strain P3HT film as understood from the morphology characterization. a) Top view of a small portion of the polymer illustrating the semicrystalline nature of the polymer of randomly oriented crystals (dark red) within an amorphous matrix (light red). The black lines are represent the polymer backbone b) Oblique view of the polymer stacking direction illustrating an edge-on morphology, which is observed for an unstrained film. c) Under strain, the polymer crystals are reorienting with the polymer backbones aligning in the direction of applied strain, while the amorphous material remaining highly disordered. d) Oblique view showing the increasing level of plane-on P3HT polymer in the alignment direction, while the crystals with the backbone initially in the direction of applied strain remaining edge-on.

mobility tensor are  $\sigma_{11} = 0.065 \text{ cm}^2 \text{V}^{-1} \text{s}^{-1} \pm 0.0017 \text{ cm}^2 \text{V}^{-1} \text{s}^{-1}$  and  $\sigma_{22} = 0.010 \text{ cm}^2 \text{V}^{-1} \text{s}^{-1} \pm 0.0017 \text{ cm}^2 \text{V}^{-1} \text{s}^{-1}$ , with the uncertainty based on standard error fit of the tensor to experimental data (off-diagonal components of the tensor are zero). The ability to fit a mobility tensor has been previously demonstrated in single-crystal organic semiconductors.<sup>[39–41]</sup> Here, we show that a mobility tensor is also applicable to semicrystalline polymer semiconductors with in-plane alignment. The value of the mobility tensor is not a direct measurement of the anisotropic crystal, but a convolution of the distribution of crystal orientations in the film as well as the amorphous material. However, the ability to apply a tensor reflects a smooth transition in transport that would not be expected with major film defects such as coarse grain boundaries, highlighting a key benefit of this alignment method.

Finally, temperature-dependent mobility measurements were performed. The mobility as a function of temperature for an unstrained film along with the orientation-dependent mobility for a 125% strained film is given in **Figure 9**. We focus on the saturated regime to minimize contact resistance effects. The mobility in the temperature range of 300 K to 150 K is fit to an Arrhenius type behavior,  $\sigma = \sigma_0 \exp(-E_a/k_b T)$ , where  $E_a$  is the activation energy,  $\sigma_0$  is the mobility prefactor,  $k_b$  is the Boltzmann constant, and  $T$  is the temperature.<sup>[1]</sup> In each case, the

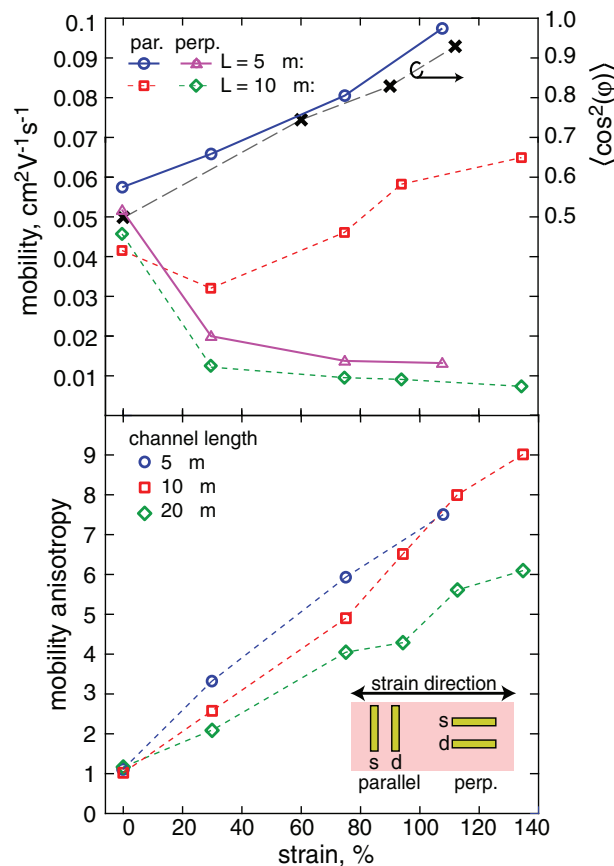


**Figure 7.** Top: saturated mobility for strain-aligned films with the transistor channel parallel and perpendicular to strain for 5 and 10 m channel lengths ( $L$ ). The average order of the (200) peak is also provided, calculated from the X-ray  $\varphi$ -scans in Figure 5 and Figure S4. Bottom: the mobility anisotropy of strain aligned P3HT films for transistors with 5, 10, and 20 m channel lengths. Inset: an illustration of the orientation of the source (s) and drain (d) electrodes relative to the direction of applied strain.

temperature dependence deviates from the fit at approximately 140 K. We find that  $E_a$  is similar in the unstrained film and in the strained film for charge transport parallel to the applied strain direction, whereas  $E_a$  is slightly higher in the strained film for transport perpendicular to the applied strain direction. These results indicate that the same limiting factor exists in transport for the isotropic film and transport parallel to the applied strain direction, while transport perpendicular to the strain direction has a unique transport bottleneck. We note that the Arrhenius fits do not include the last three temperature data points, however the temperature-dependent mobility trends are consistent over this temperature range.

Charge transport through the amorphous material that separate grains likely contributes to  $E_a$ . The similar  $E_a$  for the unstrained film and in the strained film for transport parallel to the applied strain direction suggests that the amorphous-material charge-trap distribution is similar between these films, consistent with the similar structure deduced from the morphological analysis. In addition, the relative orientation of adjacent grains can also contribute to  $E_a$ .<sup>[2]</sup> Charge percolation in

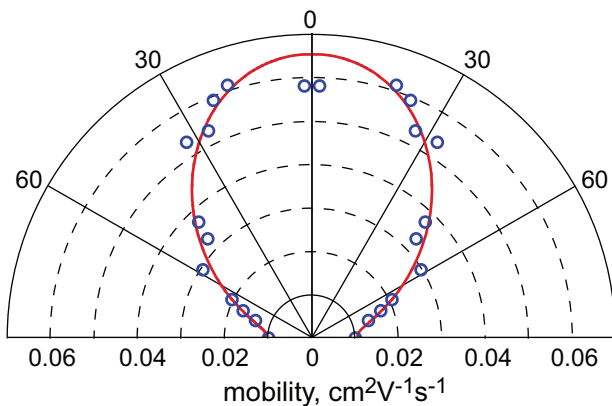


**Figure 8.** Mobility versus angle for films strained by 100%. The data is from six strained films applied to orthogonal transistors. The mobility data is reported from 0 to 90° and reflected to show the expected behavior of the mobility anisotropy over a 180° range. The semicrystalline nature of the film along with the crystalline distribution around the strain direction allows for this expectation.

favorably aligned grains of the isotropic film may be similar to percolation through the increasing number of favorable grains in the aligned film, keeping  $E_a$  similar but changing  $\sigma_0$ . The slightly higher  $E_a$  consistently observed for perpendicular transport may arise from anisotropic grain boundaries,<sup>[2]</sup> a reduction of the amount of polymer backbone aligned in the transport direction, and an increase in the amount of alkyl side chains

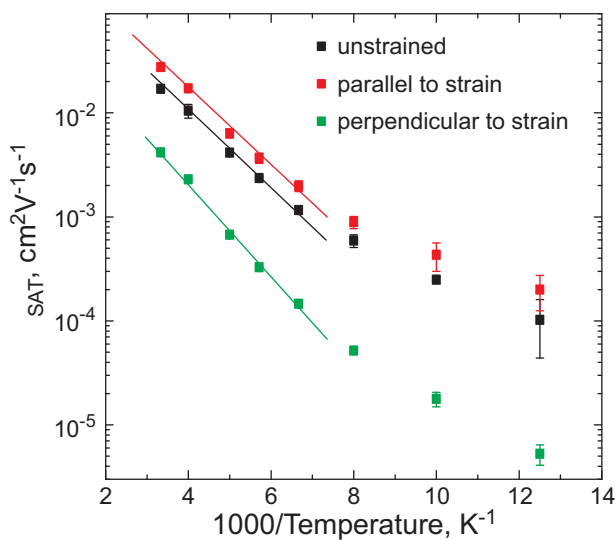


**Figure 9.** The saturated mobility for an unstrained film and a film strained by 125% with variation in temperature. The mobility for the strained film is for source-drain electrodes parallel and perpendicular to the strain direction with 10 μm channel lengths. The data are fit to an exponential over the high-temperature regime. From the exponential fit, the activation energy in this regime is 70 meV for the unstrained film, and for the strained film 71 meV parallel to the applied strain direction and 94 meV perpendicular to strain. The uncertainty in the data points is based on one standard deviation of 4 devices for the unstrained film, and 2 devices each for the parallel and perpendicular directions of the strained film.

stacking in the transport direction (where transport is believed to be efficient along the polymer backbone direction and inefficient in the alkyl stacking direction).<sup>[42]</sup> Considering charge percolation, the last two possibilities would not be expected to change  $E_a$  until the favored percolation path (the polymer backbone direction) is reduced to the point where a secondary path becomes significant. This secondary path will likely have a different  $E_a$ .

Combining the mobility results with known changes in the morphology points to several underlying features of charge transport in P3HT. For an isotropic film, the measured mobility is a result of transport through both locally anisotropic crystallites and isotropic amorphous material. For the strained films, the morphological analysis indicates that charge transport occurs through highly orientated crystalline material and weakly oriented amorphous material. This is consistent with the temperature-dependent TFT measurements that suggest similar transport characteristics for the amorphous material within both the isotropic and aligned films. In addition, there is a similar trend between mobility parallel to the strain direction and the average orientation of the polymer backbone in the crystal (Figure 5 and Figure 7), indicating a strong correlation between crystalline orientation and charge-mobility improvement. Comparatively, the order parameter based on the entire film does not correlate well with improved mobility, as shown in Figure 5. These results suggest that the improved mobility parallel to strain is primarily due to the alignment of the P3HT backbone of the crystalline material in the direction of applied strain. The improved mobility could also result from anisotropic grain boundaries assisted by the reorientation of the crystalline material and cannot be ruled out. An improvement in mobility from anisotropic grains may occur if favorable or fewer grains boundaries developed along the strain direction than existed for an isotropic film.

Critically, for a system described by a 2D tensor, the increase in  $\sigma_{11}$  from an unoriented film to a highly oriented film requires a significant difference between the two components of the tensor  $\sigma_{11}$  and  $\sigma_{22}$  [since  $\sigma_{iso} = (\sigma_{11} + \sigma_{22})/2$ ]. Extrapolating the tensor component  $\sigma_{11}$  to a completely aligned film [i.e.,  $R/(R+1) = 1$ ], results in an estimated  $\sigma_{11}$  of just greater than  $2 \times \sigma_{iso}$  for the 5 μm channel-length devices, and just under  $2 \times \sigma_{iso}$  for the 10 μm channel-length devices. Either estimate requires that  $\sigma_{11} \gg \sigma_{22}$  for hypothetical perfect orientation. Because morphological anisotropy arises from alignment of crystalline P3HT along the *c*-axis (parallel to the polymer backbone), charge mobility along the polymer backbone must therefore be far greater than charge mobility in the intermolecular π–π direction. These results agree with theoretical models that predict that charge transport along the polymer backbone is favored, followed by the π-stacking direction, and finally the alkyl-stacking direction.<sup>[1,36,42]</sup> Although our interpretation suggests that significant long-range charge transport does not occur via π–π overlap in P3HT, the overwhelming literature evidence for correlation between the extent of π–π overlap and charge mobility leads us to believe that π–π interactions remain a critical aspect of P3HT local packing, perhaps for ensuring backbone planarity and circumventing traps. Alternatively, tie chains in this material system may play a critical role in charge transport and therefore the relative orientation of the tie chains may have a significant

effect on mobility anisotropy.<sup>[42]</sup> If tie chains dominate charge transport, the results would be consistent with the temperature-dependent mobility and tensor representation of mobility.

Finally, the increase in mobility along the applied strain direction also indicates that charge transport along the polymer backbone is efficient for both edge-on and plane-on packing motifs; the unstrained film is highly edge-on and the strained films have a substantial plane-on fraction. This secondary result supports our interpretation of the anisotropic transport above. Although  $\pi$ - $\pi$  interactions may be a key part of ensuring local P3HT chain order, they may not be a high-mobility mechanism for long-range charge transport within a P3HT film.

### 3. Conclusions

Combining the mobility results with the known changes in the morphology illuminates several key features of charge transport in P3HT. Mobility increases in the direction of backbone alignment suggesting significantly favored transport along the polymer backbone over  $\pi$ - $\pi$  intermolecular transport. The anisotropy that develops may also include contributions from anisotropic grain boundaries and/or relative tie chain orientation, however the similar trend between the increase in mobility and the average crystal orientation suggests that the change in mobility parallel to the strain direction is dictated most significantly by the on-crystal mobility anisotropy of P3HT. This conclusion is consistent with theoretical predictions that the mobility along the polymer backbone is more than one order of magnitude greater than the mobility in the  $\pi$ - $\pi$  direction within a P3HT crystal.<sup>[42]</sup> The strain alignment is found to induce significant face-on orientation of the originally highly edge-on oriented crystalline regions of the film, and the mobility parallel to the backbone is shown to be high for both plane-on and edge-on packing configurations. This result is consistent with our conclusion that charge transport along the polymer backbone is dominant. The charge mobility in the strained films is successfully represented by a 2D tensor, highlighting a continuous film with no major defects responsible for the mobility anisotropy. Finally, it is important to highlight that these features of charge transport were made possible through the development of a simple but powerful strain-alignment procedure that is able to align the polymer without compromising film quality.

### 4. Experimental Section

**Film Preparation:** P3HT is dissolved into chloroform at approximately 8 mg mL<sup>-1</sup>. The P3HT was obtained from Plextronics Inc. with a number-average molecular mass  $M_n = 62$  kD, a regioregularity of 99%, and a polydispersion of 1.9 measured by gel permeation chromatography (GPC).<sup>[43]</sup> The P3HT solution is spun cast at room temperature with a spinning rate of 1000(2 $\pi$ /60) rad s<sup>-1</sup> (i.e., 1000 rpm) for 45 s onto OTS-treated silicon substrates with a native oxide layer. The OTS treatment followed a previously described process<sup>[44]</sup>

**Film Alignment:** The P3HT film on octyltrichlorosilane-modified silicon substrate with a native oxide layer (OTS-Si) is laminated to a PDMS slab and the substrate is pulled off leaving behind the P3HT film on the PDMS. The NEXAFS results show that the OTS layer remains on the Si during this process (see the Supporting Information). The

P3HT-PDMS composite is then strained to varying extents and held in place and a second substrate with an oxidized surface is laminated to the P3HT film. The strained PDMS is then removed, leaving behind the P3HT film on the second substrate. During the strain process PDMS is elastically deformed while the P3HT undergoes plastic deformation. The secondary substrates include a glass (0215 Corning glass slide) and a silicon wafer with either a native or 230-nm thermal oxide layer. All substrates were cleaned by sonication in acetone, isopropyl alcohol, and de-ionized water prior to further processing. Prior to P3HT film transfer, these substrates were all placed in a UV-ozone chamber for 10 min and rinsed with deionized water. The PDMS was approximately 2 mm thick, cast with a cross-linker concentration of 20:1, and cured at a temperature of 60 °C overnight.

**Morphology Characterization:** The UV-vis absorbance measurements were performed with a Perkin Elmer Lambda 950 UV-vis-near-IR spectrometer. X-ray diffraction was performed at the Stanford Synchrotron Radiation Lightsource (SSRL) on beam lines 7-2 and 11-3. The point detector GIXD measurements were conducted on beam line 7-2. The films were illuminated with an 8 keV beam at a constant incidence angle of approximately 0.2°. The sample in-plane orientation relative to the beam was adjusted at each  $q$ -value to maintain the scattering vector parallel or perpendicular to the strain direction. For  $\varphi$ -scans, the sample tilt was adjusted to make the sample normal collinear with the rotation axis of the  $\varphi$  motor and maintain a constant incidence angle as the sample was rotated. The 2D GIXD measurements were conducted on beam line 11-3 with an area detector (MAR345 image plate), an energy of 12.735 keV, and an incidence angle of  $\approx 0.12$ . For area detector measurements, the samples were aligned with their in-plane orientation either perpendicular or parallel to the *incident beam*. This orientation resulted in the scattering vector being aligned away from the strain direction by  $\theta_B$ . For the energy used,  $\theta_B$  was 3.3° for the (200) and 7.3° for the (010) scattering peaks, both less than the FWHM observed in the  $\varphi$ -scans. All sample chambers were purged with helium during the scattering experiments to reduce beam damage and background scattering. Spectroscopic ellipsometry measurements were performed with an M 2000 series ellipsometer (J.A. Woollam Co., Inc.) and analyzed using vendor-supplied software in a previously described method.<sup>[45]</sup> The thickness of the cast films measures by ellipsometry were approximately 80 nm. AFM measurements were performed on an Asylum MFP3D in intermittent-contact mode.

**Electrical Characterization:** For electrical characterization, the film was transferred from the PDMS to Fraunhofer Inc. transistor test structures that consisted of a 230 nm SiO<sub>2</sub> gate dielectric on a highly doped Si wafer with source-drain electrodes that consisted of a 30 nm Au and a 10 nm indium tin oxide adhesion layer patterned by lift-off. The channel widths for all devices were 10  $\mu$ m while the channel lengths included 5, 10, and 20  $\mu$ m. The transistors were measured using an HP 4156b parameter analyzer. Room-temperature TFTs were measured in the saturated regime by sweeping the gate voltage ( $V_g$ ) from -20 to 60 V, with a source-drain voltage ( $V_{SD}$ ) of 80 V. Low-temperature measurements were performed with a Desert Inc. cryogenic probe station in the saturation regime, with  $V_g$  swept from -20 to 60 V and  $V_{SD} = 60$  V. Low-temperature measurements were conducted at a pressure of approximately  $1.3 \times 10^{-6}$  Pa ( $10^{-8}$  Torr). The saturated field-effect hole mobility was calculated from a linear fit of  $I_{sd}^{1/2}$  versus  $V_g$ , where  $I_{sd}$  is the source-drain current.

Initial polymer processing was performed in a nitrogen environment, AFM, VASE, UV-vis spectroscopy measurements were carried out in atmosphere, NEXAFS was conducted in vacuum, XRD measurements were performed in a He-rich atmosphere, room-temperature transistor measurements were performed in a argon-filled glove box, and low-temperature transistor measurements were performed in vacuum at approximately  $10^{-8}$  Torr. It is also worth noting that transistor measurements were carried out both in air and in vacuum without significant changes in performance, highlighting the intimate contact made between the P3HT film and both the transistor dielectric layer and the source-drain electrodes after the transfer process.

## Supporting Information

Supporting Information is available from the Wiley Online Library or from the author.

## Acknowledgements

Portions of this research were carried out at the Stanford Synchrotron Radiation Lightsource, a national user facility operated by Stanford University on behalf of the U.S. Department of Energy, Office of Basic Energy Sciences. The authors would like to thank Edwin Chan and Peter Johnson for helpful conversations. B.O'C. and B.C. would like to acknowledge the NIST National Research Council Postdoctoral Fellowship Program. Support from C.L. Soles and the Electronic Materials Group NIST Polymers Division is also acknowledged.

Received: April 22, 2011  
Published online: August 16, 2011

- [1] R. A. Street, J. E. Northrup, A. Salleo, *Phys. Rev. B* **2005**, *71*, 165202.
- [2] L. H. Jimison, M. F. Toney, I. McCulloch, M. Heeney, A. Salleo, *Adv. Mater.* **2009**, *21*, 1568.
- [3] D. M. DeLongchamp, R. J. Kline, Y. Jung, D. S. Germack, E. K. Lin, A. J. Moad, L. J. Richter, M. F. Toney, M. Heeney, I. McCulloch, *ACS Nano* **2009**, *3*, 780.
- [4] J. Rivnay, L. H. Jimison, J. E. Northrup, M. F. Toney, R. Noriega, S. F. Lu, T. J. Marks, A. Facchetti, A. Salleo, *Nat. Mater.* **2009**, *8*, 952.
- [5] C. W. Sele, B. K. C. Kjellander, B. Niesen, M. J. Thornton, J. van der Putten, K. Myny, H. J. Wondergem, A. Moser, R. Resel, A. van Breemen, N. van Aerle, P. Heremans, J. E. Anthony, G. H. Gelinck, *Adv. Mater.* **2009**, *21*, 4926.
- [6] Z. J. Zheng, K. H. Yim, M. S. M. Saifullah, M. E. Welland, R. H. Friend, J. S. Kim, W. T. S. Huck, *Nano Letters* **2007**, *7*, 987.
- [7] Z. J. Hu, B. Muls, L. Gence, D. A. Serban, J. Hofkens, S. Melinte, B. Nyström, S. Demoustier-Champagne, A. M. Jonas, *Nano Letters* **2007**, *7*, 3639.
- [8] C. J. Yu, J. H. Bae, C. M. Keum, S. D. Lee, *Curr. Appl. Phys.* **2010**, *10*, 64.
- [9] H. Sirringhaus, R. J. Wilson, R. H. Friend, M. Inbasekaran, W. Wu, E. P. Woo, M. Grell, D. D. C. Bradley, *Appl. Phys. Lett.* **2000**, *77*, 406.
- [10] L. R. Pattison, A. Hexemer, E. J. Kramer, S. Krishnan, P. M. Petroff, D. A. Fischer, *Macromolecules* **2006**, *39*, 2225.
- [11] L. Kinder, J. Kanicki, P. Petroff, *Synth. Met.* **2004**, *146*, 181.
- [12] S. H. Jin, H. U. Seo, D. H. Nam, W. S. Shin, J. H. Choi, U. C. Yoon, J. W. Lee, J. G. Song, D. M. Shin, Y. S. Gal, *J. Mater. Chem.* **2005**, *15*, 5029.
- [13] K. R. Amundson, B. J. Sapjeta, A. J. Lovinger, Z. N. Bao, *Thin Solid Films* **2002**, *414*, 143.
- [14] M. J. Banach, R. H. Friend, H. Sirringhaus, *Macromolecules* **2003**, *36*, 2838.
- [15] M. J. Banach, R. H. Friend, H. Sirringhaus, *Macromolecules* **2004**, *37*, 6079.
- [16] A. Bolognesi, C. Botta, C. Mercogliano, W. Porzio, P. C. Jukes, M. Geoghegan, M. Grell, M. Durell, D. Trolley, A. Das, J. E. Macdonald, *Polymer* **2004**, *45*, 4133.
- [17] A. Bolognesi, C. Botta, C. Mercogliano, M. Marinelli, W. Porzio, L. Angiolini, E. Salatelli, *Polym. Adv. Technol.* **2003**, *14*, 537.
- [18] H. Heil, T. Finnberg, N. von Malm, R. Schmeichel, H. von Seggern, *J. Appl. Phys.* **2003**, *93*, 1636.
- [19] M. Brinkmann, J. C. Wittmann, *Adv. Mater.* **2006**, *18*, 860.
- [20] M. Brinkmann, P. Rannou, *Adv. Funct. Mater.* **2007**, *17*, 101.
- [21] Y. F. Tao, H. Zohar, B. D. Olsen, R. A. Segelman, *Nano Letters* **2007**, *7*, 2742.
- [22] T. G. Backlund, H. G. O. Sandberg, R. Osterbacka, H. Stubb, M. Torkkeli, R. Serimaa, *Adv. Funct. Mater.* **2005**, *15*, 1095.
- [23] T. Yasuda, L. Y. Han, T. Tsutsui, *J. Photopolym. Sci. Technol.* **2009**, *22*, 713.
- [24] C. Y. Yang, C. Soci, D. Moses, A. J. Heeger, *Synth. Met.* **2005**, *155*, 639.
- [25] T. M. S. Wilson, D. A. Chinn, D. B. Robinson, F. P. Doty, *Appl. Phys. Lett.* **2008**, *93*, 143304.
- [26] E. K. Miller, D. Yoshida, C. Y. Yang, A. J. Heeger, *Phys. Rev. B* **1999**, *59*, 4661.
- [27] P. Dyreklev, G. Gustafsson, O. Inganäs, H. Stubb, *Solid State Commun.* **1992**, *82*, 317.
- [28] P. Dyreklev, O. Inganäs, *Synth. Met.* **1995**, *69*, 387.
- [29] J. A. DeAro, D. Moses, S. K. Buratto, *Appl. Phys. Lett.* **1999**, *75*, 3814.
- [30] S. Nagamatsu, W. Takashima, K. Kaneto, Y. Yoshida, N. Tanigaki, K. Yase, *Macromolecules* **2003**, *36*, 5252.
- [31] W. Y. Chou, H. L. Cheng, *Adv. Funct. Mater.* **2004**, *14*, 811.
- [32] M. L. Chabinyc, A. Salleo, Y. L. Wu, P. Liu, B. S. Ong, M. Heeney, I. McCulloch, *J. Am. Chem. Soc.* **2004**, *126*, 13928.
- [33] R. J. Kline, M. D. McGehee, M. F. Toney, *Nat. Mater.* **2006**, *5*, 222.
- [34] M. C. Gurau, D. M. Delongchamp, B. M. Vogel, E. K. Lin, D. A. Fischer, S. Sambasivan, L. J. Richter, *Langmuir* **2007**, *23*, 834.
- [35] J. Clark, C. Silva, R. H. Friend, F. C. Spano, *Phys. Rev. Lett.* **2007**, *98*.
- [36] H. Sirringhaus, P. J. Brown, R. H. Friend, M. M. Nielsen, K. Bechgaard, B. M. W. Langeveld-Voss, A. J. H. Spiering, R. A. J. Janssen, E. W. Meijer, P. Herwig, D. M. de Leeuw, *Nature* **1999**, *401*, 685.
- [37] T. Sauer, T. Arndt, D. N. Batchelder, A. A. Kalachev, G. Wegner, *Thin Solid Films* **1990**, *187*, 357.
- [38] A. Zen, M. Saphiannikova, D. Neher, J. Grenzer, S. Grigorian, U. Pietsch, U. Asawapirom, S. Janietz, U. Scherf, I. Lieberwirth, G. Wegner, *Macromolecules* **2006**, *39*, 2162.
- [39] O. Ostroverkhova, D. G. Cooke, F. A. Hegmann, R. R. Tykwiński, S. R. Parkin, J. E. Anthony, *Appl. Phys. Lett.* **2006**, *89*, 192113.
- [40] V. C. Sundar, J. Zaumseil, V. Podzorov, E. Menard, R. L. Willett, T. Someya, M. E. Gershenson, J. A. Rogers, *Science* **2004**, *303*, 1644.
- [41] C. Reese, Z. Bao, *Adv. Mater.* **2007**, *19*, 4535.
- [42] Y. K. Lan, C. I. Huang, *J. Phys. Chem. B* **2009**, *113*, 14555.
- [43] Certain commercial equipment, or materials are identified in this paper in order to specify the experimental procedure adequately. Such identification is not intended to imply recommendation or endorsement by the National Institute of Standards and Technology, nor is it intended to imply that the materials or equipment identified are necessarily the best available for the purpose.
- [44] R. J. Kline, D. M. DeLongchamp, D. A. Fischer, E. K. Lin, M. Heeney, I. McCulloch, M. F. Toney, *Appl. Phys. Lett.* **2007**, *90*, 062117.
- [45] D. M. DeLongchamp, R. J. Kline, D. A. Fischer, L. J. Richter, M. F. Toney, *Adv. Mater.* **2010**, *23*, 319.